

# Development of Multilayered Coatings for NERVA-Type Graphite Fuel Elements—An Overview

S. V. Raj<sup>1</sup>

<sup>1</sup>NASA Glenn Research Center, MS 106-5, 21000 Brookpark Road, Cleveland, OH, 44135

Primary Author Contact Information: Tel.: (216) 433 8195; e-mail: sai.v.raj@nasa.gov

[Placeholder for Digital Object Identifier (DOI) to be added by ANS]

*“Mid-passage corrosion” (MPC) was observed in NbC and ZrC-coated graphite (Gr)-based nuclear fuels during the NERVA/Rover programs. A new multilayered coating concept was proposed to solve this problem. The concept envisions designing a compliant multilayered coatings architecture to accommodate the thermal expansion mismatch strains between the ZrC outer coating and the Gr/(U,Zr)C fuel matrix. Additionally, the coating architecture uses diffusion barriers to minimize carbon diffusion from the substrate, and hydrogen diffusion from the flowing gas stream, into the multilayer coating. The present paper provides a brief overview of the development of multilayered coatings deposited on Gr disks, as well as within the inner channels of a 19-hole 152.4 mm long hexagonal rod, by chemical vapor deposition (CVD) in proof-of-concept studies. The cross-sectional microstructural observations are discussed. These trials have established that it is possible to deposit multilayered coatings by CVD in 19-hole hexagonal rods similar to the NERVA fuel rod design although the quality of the coatings and the uniformity of their thicknesses require further improvement.*

## I. INTRODUCTION

Several ground tests conducted during the Nuclear Engine for Rocket Vehicle Application (NERVA) and Rover programs between 1959 and 1972 demonstrated the viability of using coated UC/Gr nuclear fuel elements in NTP engines.<sup>1,2</sup> These extruded (U,Zr)C/Gr nuclear fuel rods had 19 channels, which were coated with either NbC or ZrC using chemical vapor deposition (CVD).<sup>3-7</sup> The NTP engine lives were severely limited by “mid-passage” corrosion (MPC) of the graphite (Gr)-based nuclear fuel, where cracks that had formed in the coatings during cool down from the CVD temperatures allowed the hot hydrogen propellant to react with the Gr substrate to form hydrocarbon reaction products.<sup>6-10</sup> The formation of these cracks were attributed to differences in the coefficients of thermal expansion (CTE) between the carbide coating and the (U,Zr)C/Gr substrate.<sup>6,7</sup> A new multilayer coating architecture was proposed to address this MPC problem.<sup>11-17</sup> The present paper describes a brief overview of the developmental research conducted at NASA’s Glenn Research Center (GRC), Cleveland, OH on depositing this multilayered-coating architecture on Gr disk and hexagonal rod substrates.

## 1.A. Multilayer Coating Architecture

Figure 1 is a schematic of the multilayered coating architecture, (U,Zr)C-Gr/NbC (or ZrC) diffusion barrier/Mo/Nb/ZrC/Mo overlayer, developed by GRC.<sup>11-17</sup> Details of the requirements of the coating architecture are discussed in Ref. 14. The proposed architecture consists of a NbC (or a ZrC) diffusion barrier layer next to the Gr substrate to minimize the outward diffusion of carbon from the substrate and to fill the pores in the substrate. The Mo and Nb deposited on the NbC (or a ZrC) diffusion barrier are intended to act as strain compliant layers, where it has been demonstrated that the thermal expansion strains for several Nb-Mo alloys lie between those for Gr, NbC, and ZrC.<sup>17</sup> The top layer consists of ZrC overlaid with a Mo layer since it was demonstrated that using a Mo overlayer increased coating lives significantly.<sup>1</sup> Since hydrogen diffusion is slow in Mo and W compared to many metals, it was envisioned that this Mo overlayer over the ZrC layer would act to minimize hydrogen diffusion into the coating. The relative ductility of the Mo during CVD deposition is expected to seal cracks that may form on the ZrC during cooling from the CVD deposition temperature.

Before the effectiveness of the proposed multilayered coating architecture in preventing or minimizing MPC can be verified, it was necessary to demonstrate in proof-of-concept studies that it was possible to deposit the complex coating architecture using CVD. Thus, a multi-step coatings development roadmap was formulated. The first step was to identify the essential process parameters and methodologies necessary to deposit the multilayer coatings on Gr disks. These process parameters and methodologies were then refined to coat the hexagonal rods. In the second step, the developmental process was extended to coating 19 channels,

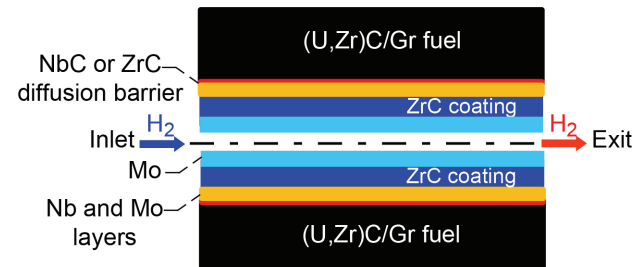


**Fig. 1.** Schematic of the multilayered coating architecture proposed to protect Gr-based nuclear fuels from hot hydrogen attack.<sup>17</sup>

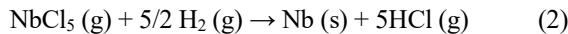
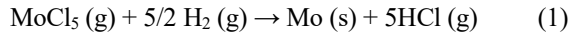
each 2.3 mm dia., machined in hexagonal Gr rods 152.4 mm long identical in dimensions to the NERVA/Rover fuel elements. The third step consisted of coating longer hexagonal rods 304.8 mm long.

The present paper summarizes the results of detailed characterization work conducted at GRC on multilayered coated Gr disks and the 152.4 mm long coated hexagonal rod to demonstrate the feasibility of depositing the proposed multilayered coatings.<sup>17</sup> It is important to note that this developmental investigation was conducted on a limited budget before the project ended. Therefore, the CVD process parameters were not optimized.

## II. COATING DEPOSITION

A contract was issued to Ultramet, Pacoima, CA to develop CVD process methodologies and parameters required to deposit this coating architecture in proof-of-concept studies in collaboration with GRC researchers. The graphite substrates used in these studies were commercially available Mersen 2160 procured as disk and hexagonal rods with a CTE of  $6.0 \times 10^{-6}/\text{K}$ .<sup>18</sup> The disk specimens were 25.4 mm dia. x 3.2 mm thick, while the 152.4 mm long hexagonal rods with 19.05 mm flat-to-flat width and 19 machined channels each 2.3 mm dia. were similar to the NERVA/ Rover fuel elements in cross-section<sup>6</sup> (Fig. 2). The  $R_a$  surface finish was 64  $\mu\text{m}$ .

Niobium pentachloride was deposited on the Gr substrates by CVD and directly reacted with the Gr to form the NbC diffusion barrier. The subsequent Mo, Nb, and the ZrC layers, as well as the Mo overlayer, were formed by the following reactions:



The disk specimens were coated in batches of approximately four specimens per batch. A total of six batches of disks were coated.



**Fig. 2.** Photograph of the Mersen 2160 hexagonal rod with 19 machined channels.<sup>17</sup>

## III. CHARACTERIZATION OF COATED DISKS

### III.A. Microstructural Characterization of As-Coated Disks

Figures 3(a-b) show the low and high magnification backscattered electron (BSE) images of the cross-sectional microstructures of a coated disk from one of the batches. It is evident that all the layers are intact except for the Mo overlay layer, which had debonded due to a high oxygen content as evident in the oxygen peak observed in the EDS result (Fig. 3(c)). A close examination of the ZrC layer revealed a two-phase lamellar microstructure within the inner 50 to 60  $\mu\text{m}$  thickness region before becoming homogeneous in the outer 8 to 10  $\mu\text{m}$  layer (Fig. 3(b)). Presumably, the partial pressures of  $\text{C}_x\text{H}_y(\text{g})$  and  $\text{ZrCl}_4(\text{g})$ , and the temperature conditions, appeared to have corresponded to the  $\text{ZrC} + \text{C} +$  gaseous region of the CVD pseudobinary phase diagram thereby resulting in a ZrC/C lamellar microstructure.<sup>19</sup>

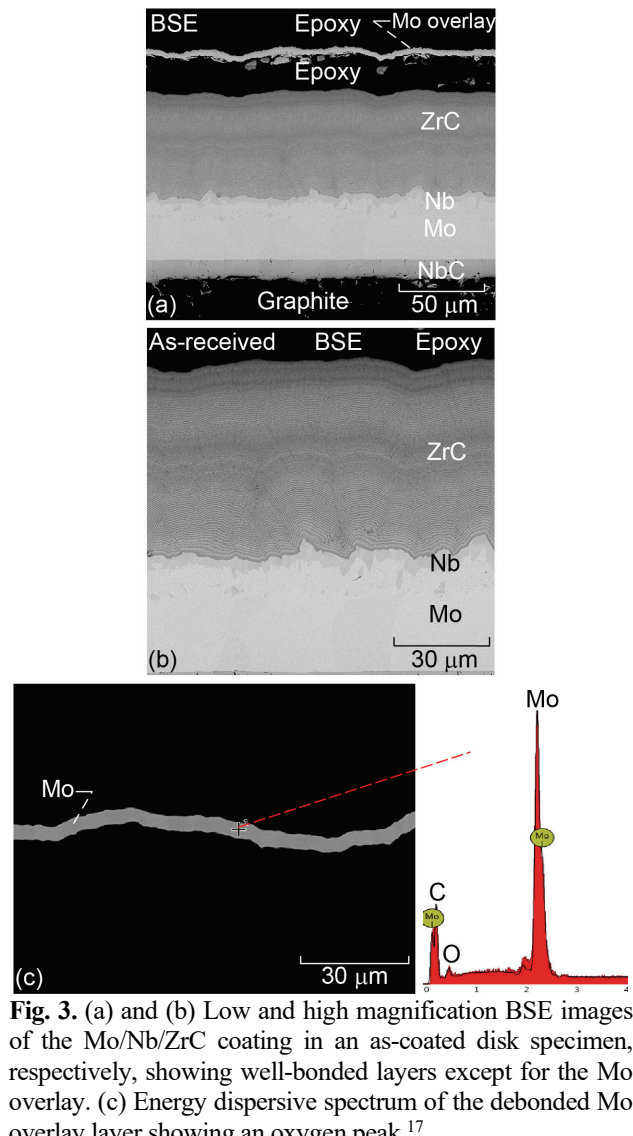


**Fig. 3.** (a) and (b) Low and high magnification BSE images of the Mo/Nb/ZrC coating in an as-coated disk specimen, respectively, showing well-bonded layers except for the Mo overlay. (c) Energy dispersive spectrum of the debonded Mo overlay layer showing an oxygen peak.<sup>17</sup>

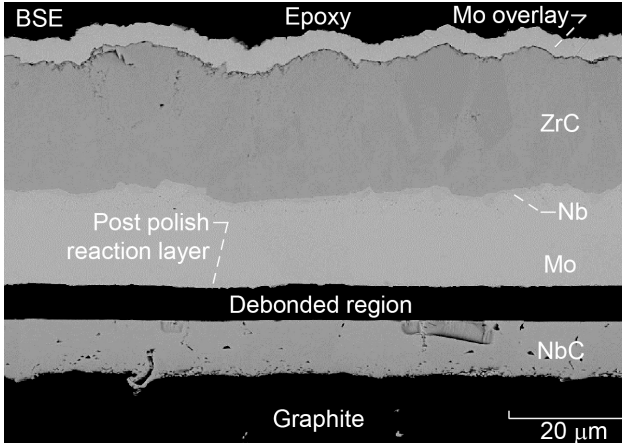


**Fig. 4.** Backscattered electron image of the cross-sectional microstructures from different locations of the as-coated disk specimen showing that all the layers except the NbC/Mo interface were well-bonded.<sup>17</sup>

In contrast, a second disk obtained from a different coated batch revealed that the Mo overlay coating was bonded to the ZrC. Instead, the NbC diffusion barrier/Mo interface had debonded near the Gr substrate (Fig. 4).

### III.B. Microstructural Characterization of Thermally-Cycled Coated Disks

Monotonic and step thermal cycling tests were conducted on the multilayered coated disks between ambient temperature and 1900 K in a vacuum furnace maintained at vacuum levels of  $1.3 \times 10^{-4}$  and  $1.3 \times 10^{-3}$  Pa., where the specimens were held at temperature for 1 h. The monotonic thermal cycling tests were conducted on another specimen coated along with the disk for which the as-received microstructures are shown in Figs. 3(a-c). Thus, the as-coated microstructure is expected to be similar to those shown in Figs. 3(a-c). Step thermal cycling tests were conducted on the second disk with the bonded Mo overlay layer but with a debonded NbC diffusion barrier/Mo interface (Fig. 4). Details of these tests and the microstructural results are described in Ref. 17.

#### III.B.1. Microstructural Observations after the Monotonic Thermally Cycling Test

In the monotonic cyclic tests, the specimen was cycled for 20 cycles. Microstructural observations of this specimen showed extensive Kirkendall porosity in the ZrC layer presumably due to the diffusion of Zr from ZrC towards the Nb layer and debonding of the ZrC/Nb interface (Figs. 5(a) & (b)). There was no significant damage in the Nb, Mo and NbC layers that could unambiguously be attributed to the effects of thermal cycling. A few transverse cracks present in the ZrC layer in the as-received specimen had propagated from the ZrC layer to the Gr substrate during thermal cycling of the specimen after 20 cycles (Fig. 5(b)). Spot energy dispersive spectral (EDS) analyses of the Nb, Mo and NbC

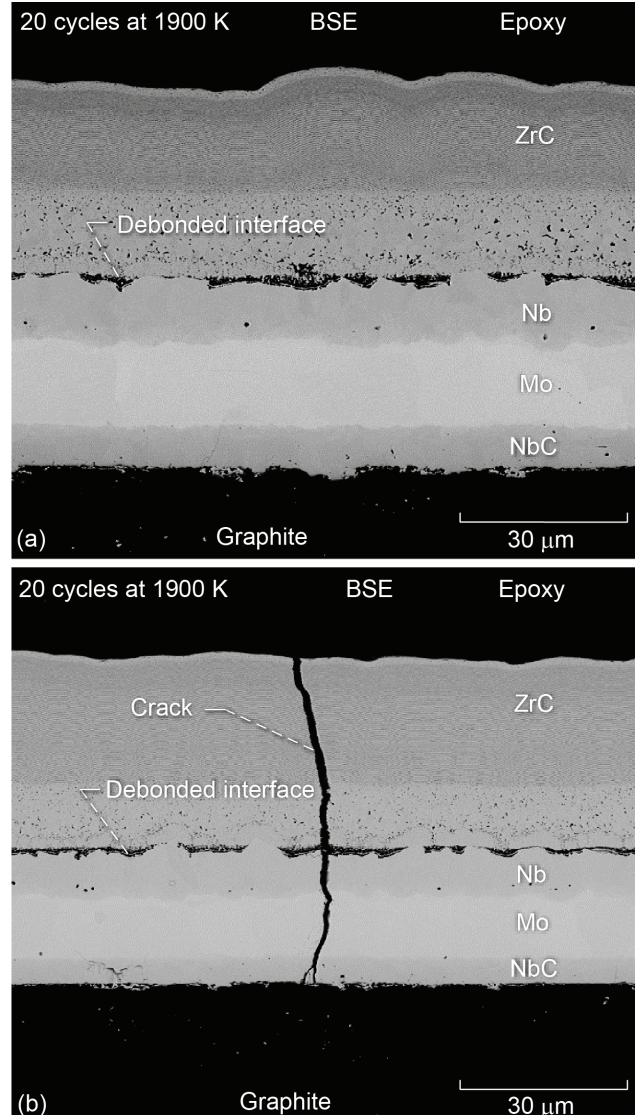


**Fig. 5.** Backscattered scanning electron images of two different regions of a specimen after thermal cycling between ambient and 1900 K for 20 cycles with a 1 h hold time. (a) Large amounts of voids were observed in the ZrC layer. (b) Transverse cracks initially observed in the ZrC layer in the as-received specimen had propagated to the Gr substrate.<sup>17</sup>

layers revealed the presence of 5.5 at.% Zr in the Nb layer. Interestingly, the Zr had also diffused into the Mo layer with the values decreasing from 3.1 at.% near the Nb layer to 2.1 at.% near the NbC layer.

#### III.B.2. Microstructural Observations after the Step Thermally Cycling Tests

The specimen used in the step-cycling tests was cumulatively cycled for 19 cycles with metallographic specimens cut for microstructural observations after each 100 K increase in temperature between 1000 and 1900 K. Figures 6(a-f) show the progressive changes in the

microstructures after stepped thermal cycling (Fig. 6(a)). Since the crack morphologies in Figs. 6(b), (e) and (f) were similar to those observed in the as-received disk, it was concluded that the vertical cracks shown in these figures did not originate during thermal cycling. Compared to the as-received microstructure (Fig. 6(a)), the microstructures did not show any noticeable changes after each thermal cycling step between 1000 and 1700 K (Figs. 6(b-d)). Vertical cracks were observed to originate at the Mo overlay/ZrC interface and propagate within the ZrC layer in the as-received coated disk.<sup>17</sup> As shown in Fig. 6(b), these vertical cracks remained in the ZrC layer and did not propagate into the Nb layer when the thermal cycling temperature was below 1700 K. In contrast, these cracks propagated through the Nb layer after testing at and above 1700 K. At 1700 K, the vertical cracks previously observed in the ZrC layer had partially propagated into the Nb layer (Fig. 6(e)) with complete penetration of the Nb layer above 1700 K (Fig. 6(f)). However, the cracks did not propagate into the Mo layer after one thermal cycle at 1900 K. Complete penetration of the Mo and the NbC diffusion layers were observed after nine additional thermal cycles at 1900 K. Although some cracks were observed in the NbC diffusion layer in the as-received microstructure (Fig. 6(a)), thermal cycling at and above 1700 K resulted in several cracks initiating and propagating in the NbC layer parallel and perpendicular to the NbC/Mo interface (Figs. 6(e-f)). Significantly, the Mo overlay did not debond and the cracks did not penetrate it.

Unfortunately, the remanent specimen had not been dried for sufficient length of time after each metallographic sectioning step prior to reintroduction into the furnace for the next thermal cycle. As a result, there was significant outgassing during heat-up to the thermal cycling temperature. Post-step thermal cycle spot EDS analyses revealed high levels of oxygen in each coating layer (Fig. 7). It is unclear the extent to which the oxygen contamination may have influenced the post-thermal cycle microstructures. The measured values of carbon are suspect as they could have been affected by hydrocarbon contamination in the SEM chamber.

#### IV. MICROSTRUCTURAL CHARACTERIZATION OF THE COATED HEXAGONAL RODS

Micro-computed tomography ( $\mu$ -CT) scans conducted on the coated rods from both ends up to a distance of 25.4 mm revealed that all the 19 channels were coated (Figs. 8(a-b)). Some of the channels had thicker coatings presumably due to higher gas mass flow rates and/or higher temperatures (Fig. 8(a)). There was no evidence of coating debonding in these images and the individual layers could not be discerned since the atomic numbers of Mo (42), Nb (41) and Zr (40) are very close.<sup>20</sup> In contrast, coating debonding was observed in a few channels in Fig. 8(b).

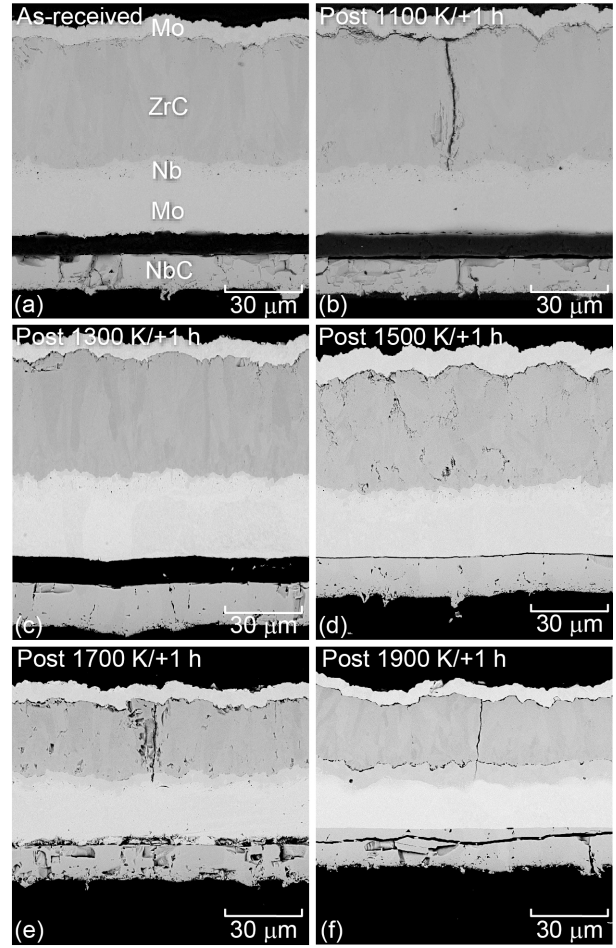


**Fig. 6.** Backscattered scanning electron images of the cross-sectional microstructures of a specimen after step thermal cycling between ambient and maximum temperatures between 1000 and 1900 K with 1 h hold times at temperature. (a) As-received; (b) 1100, (c) 1300, (d) 1500, (e) 1700, and (f) 1900 K.<sup>17</sup>

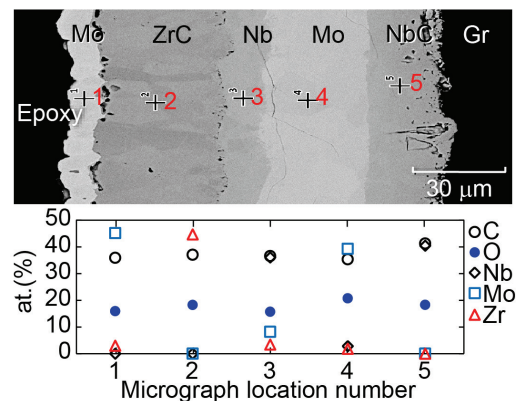


**Fig. 7.** Backscattered scanning electron image of a region of the post-step thermal cycled specimen showing the locations in each coating layer from where the EDS data were obtained. The high values of oxygen observed in all the layers are attributed to inadequate drying of the specimen after metallographic sectioning after each thermal step.<sup>17</sup>

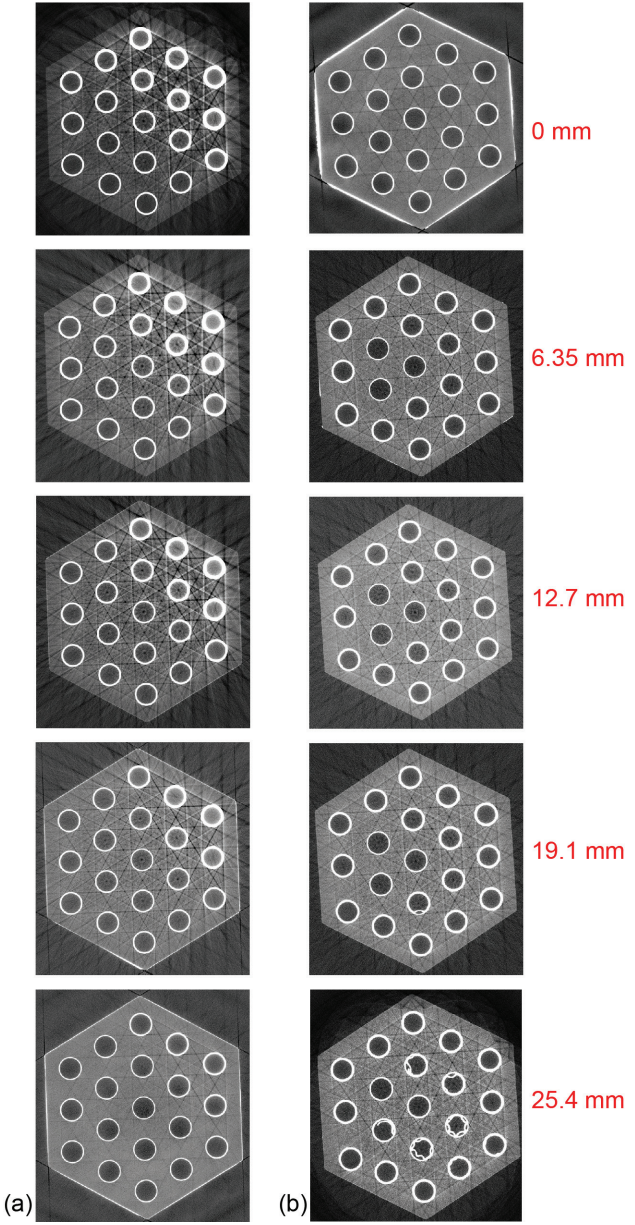


**Fig. 8.** Micro-CT scanned images obtained from the two end faces (0 mm) of the coated graphite specimen demonstrating that all the 19 channels are coated.<sup>17</sup> The images are from sections 0, 6.35, 12.7, 19.1 and 25.4 mm from each end face.

Seven transverse section almost equally spaced were sectioned from the coated hexagonal rod for microstructural examination (Figs. 9(a-g)). A total of nine channels were examined per section. Figures 10(a-c) are examples of low magnification scanning electron microscopy (SEM) images of three of these channels, 4T-1-2, 4T-3-3 and 4T-5-2, in section 4T (Fig. 9(d)). Coating debonding was observed in channels 4T-1-2 and 4T-5-2. High magnification secondary electron (SE) images revealed that the Mo overlay layer had either debonded from the ZrC layer or was absent in all three channels.<sup>17</sup>

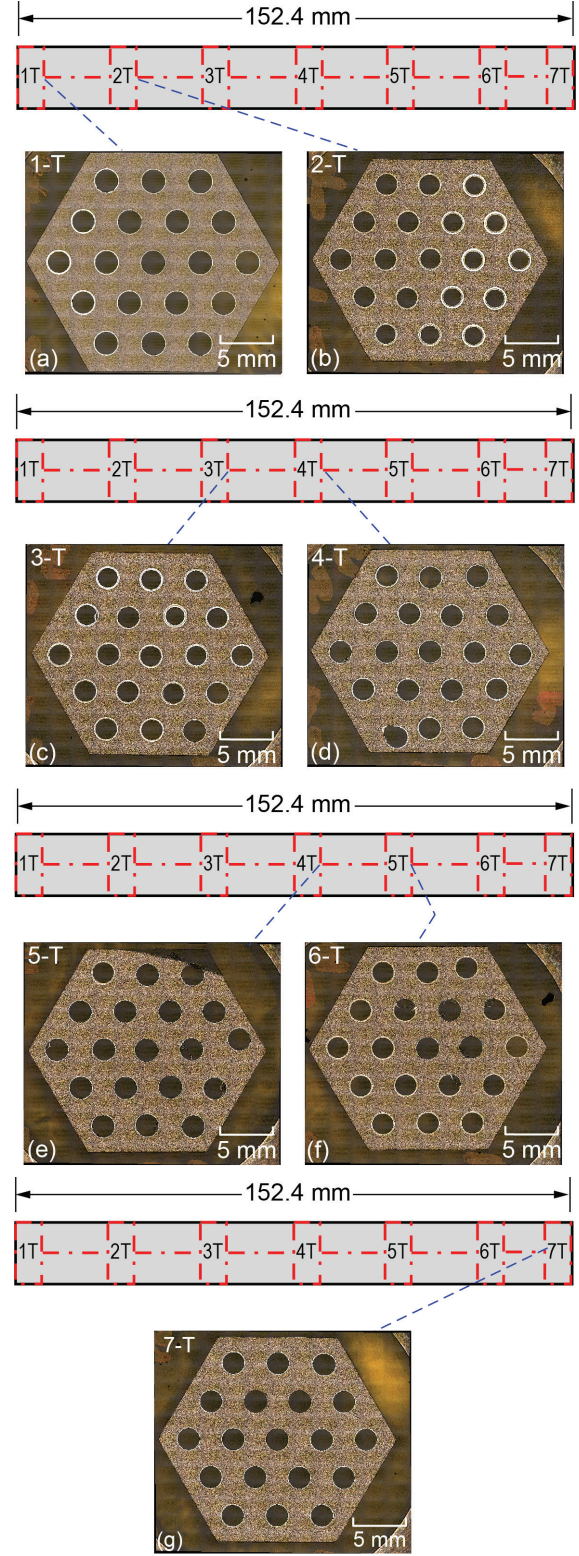


**Fig. 9.** Optical macrographs of the seven transverse sections, (a) 1T, (b) 2T, (c) 3T, (d) 4T, (e) 5T, (f) 6T and (g) 7T of the 152.4 mm long coated hexagonal rod.<sup>17</sup>

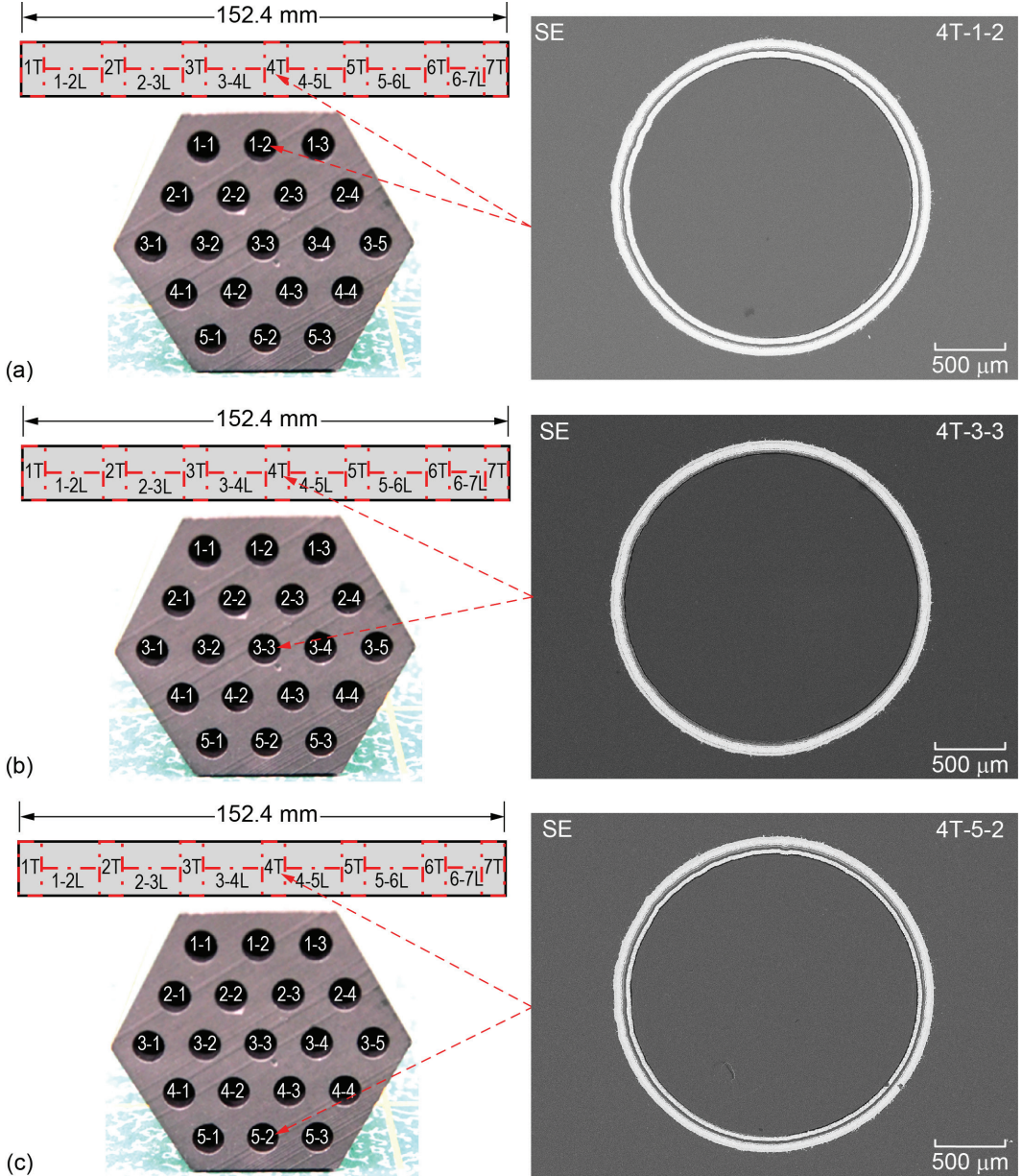


**Fig. 10.** Secondary electron images of channels (a) 4T-1-2, (b) 4T-3-3 and (c) 4T-5-2 in the transverse section 4T of the 152.4 mm long coated hexagonal rod.<sup>17</sup>

Digital x-ray elemental maps (Fig. 11(a)) and experimental line scans (Fig. 11(b)) of the coating layers in these channels confirmed the presence of C, Mo, Nb, and Zr consistent with the expected layer composition. However, the uncorrected data revealed a large amount of C in all the layers including Mo and Nb, which was attributed to contamination in the column of the scanning electron microscope. Similarly, the magnitudes of Mo, Nb and Zr were much lower than expected. After correcting for C by assuming that it was negligible in the Nb layer,<sup>17</sup> the corrected line profiles showed a reasonable compositional

profile for the major elements as well as for C although the exact stoichiometry of the NbC and ZrC could not be determined unambiguously (Fig. 11(c)). A significant amount of O (~20 at.%) observed in the Mo layers appears to have contributed to the poor bonding of the Mo overlay layer to the ZrC layer. The source of the oxygen contaminant can be attributed to either a pinhole leak in the CVD system or MoOCl<sub>3</sub> impurities in the CVD precursor MoCl<sub>5</sub> salt. It is important to minimize the O content in the coatings to trace levels in order to ensure strong bonding between the layers.

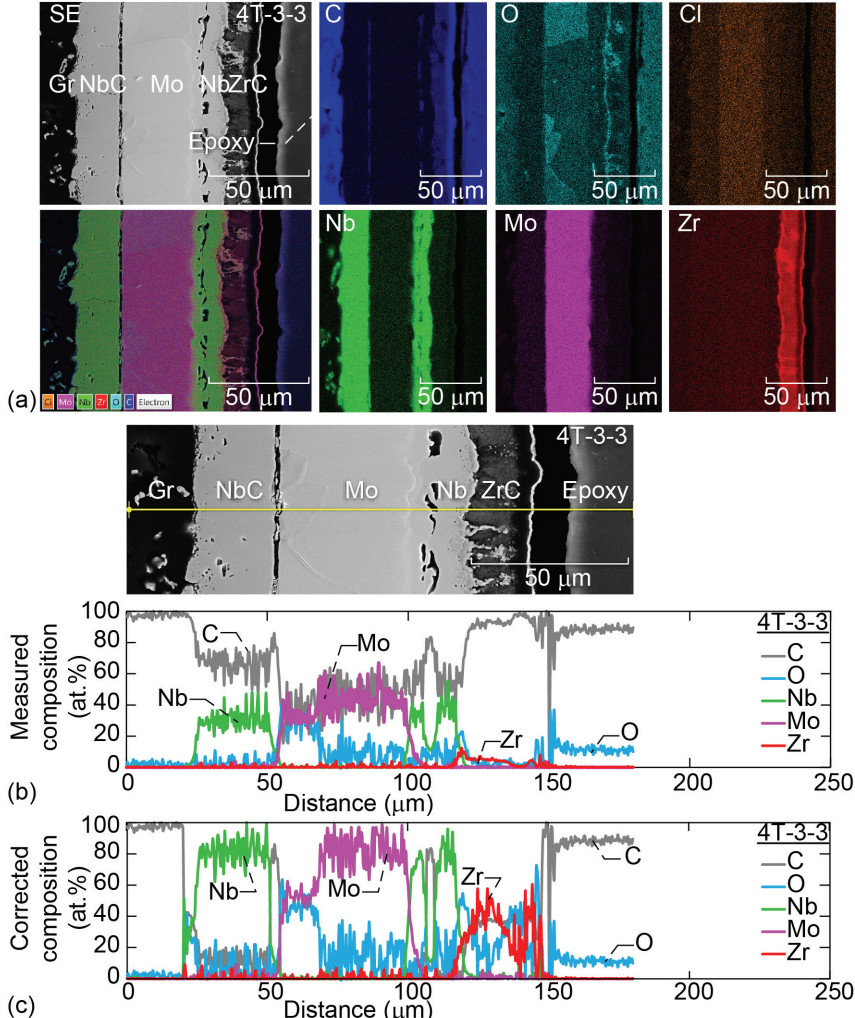


**Fig. 11.** (a) Secondary electron image and corresponding EDS maps for C, O, Nb, Mo and Zr for channel 4T-3-3. (b) Experimental line scan compositional profiles for C, O, Nb, Mo and Zr along the yellow line shown in the micrograph. (c) Corrected line scan compositional profiles of the data shown in (b) for C, O, Nb, Mo and Zr.<sup>17</sup>

## V. SUMMARY AND CONCLUSIONS

A new multilayered coating architecture was proposed to address the “mid-passage corrosion” problem observed in NERVA/Rover Gr-based nuclear fuel rods. Significantly, it was demonstrated successfully that this coating architecture can be deposited on Gr disks as well as within 19 channels, each 2.3 mm in diameter, machined in hexagonal rods 152.4 mm long. Detailed microstructural characterization of two coated disks were conducted. All the layers were well-bonded in one disk except for the Mo overlay layer, which had debonded from the ZrC layer. In this case, the EDS analysis showed significant oxygen contamination of the Mo overlay layer, which appeared to be the cause of poor bonding of the Mo overlay layer to the ZrC layer. In the second disk, while the Mo overlay layer was bonded to the ZrC layer, it was observed that NbC diffusion barrier/Mo layer had debonded. Monotonic thermal cycling tests were conducted on another disk coated under identical conditions as the disk with the debonded Mo overlay layer. These thermal cycles were

conducted between ambient and 1900 K with a 1 h hold time at temperature for 20 cycles. The second disk with the bonded Mo overlay layer was step thermally-cycled between 1000 and 1900 K, where the cycling temperature was increased in steps of 100 K from 1000 to 1900 K, for a cumulative of 19 cycles and a 1 h hold time at each temperature. Metallographic specimens were cut for microstructural observations after cycling at each temperature step. Post-test microstructural observations of the specimen tested under monotonic thermal cycling conditions revealed Kirkendall porosity in the ZrC layer presumably due to the diffusion of Zr from ZrC towards the Nb layer and debonding of the ZrC/Nb interface. In contrast, there was no significant difference between the post-test microstructures after step thermal cycles below 1700 K and those observed in the as-received specimen. Testing at and above 1700 K increased propagation of the vertical cracks initially present in the ZrC layer in the as-received specimen into the other layers towards the Gr substrate. Additionally, substantial cracking was observed in the NbC diffusion layer.

Micro-CT scans conducted on a coated 19-channel 152.4 mm long hexagonal rod revealed that all the channels were coated, which was confirmed by detailed microstructural observations conducted on seven sections along the length of the rod. These results proved for the first time that the proposed multilayered coating architecture can be deposited successfully within 19 channels in a 152.4 mm long Gr rod. It was observed that the Mo overlay layer had either debonded or it was absent in some instances. The high oxygen content observed in the Mo layers appears to have contributed to the poor bonding of the Mo overlay layer to the ZrC layer. The probable source of oxygen contamination was attributed to either a pinhole leak in the CVD system or MoOCl<sub>3</sub> impurities in the CVD precursor MoCl<sub>5</sub> salt.

## ACKNOWLEDGMENTS

The author thanks his collaborators Dr. James Nesbitt, Dr. Wayne Jennings, Dr. Peter Bonacuse, Mr. Rick Rauser, and Mr. Victor Arrieta and Mr. Brian Williams of Ultramet for their contributions. Mr. Daniel Falkenbach reviewed this paper and his comments are gratefully acknowledged. The coatings were deposited at Ultramet, Pacoima, CA under contract with GRC. This work was supported by NASA's Space Technology Mission Directorate (STMD) through the Space Nuclear Propulsion (SNP) project.

## REFERENCES

1. M. J. L. TURNER, "Rocket and Spacecraft Propulsion: Principles, Practice and New Developments," pp. 197-247, 2nd ed., Springer/Praxis Publishing, Chichester, UK (2005).
2. K. BENENSKY, "Tested and Analyzed Fuel Form Candidates for Nuclear Thermal Propulsion Applications," Nuclear Engineering Reports, University of Tennessee, Knoxville, TN, (2016). [https://trace.tennessee.edu/utne\\_reports/5](https://trace.tennessee.edu/utne_reports/5).
3. T. C. WALLACE, "Chemical Vapor Deposition of ZrC in Small Bore Carbon-Composite Tubes," LA-UR-73-692, Los Alamos National Laboratory, Los Alamos, NM (1973).
4. A. J. CAPUTO, "Characterization of Vapor-Deposited Niobium and Zirconium Carbides," Nerva Fuel Element Development Program, Summary Report - July 1966 through June 1972, Y1852 Part 3," Oak Ridge Y-12 Plant, Oak Ridge, TN, September (1973).
5. A. J. CAPUTO, "Vapor Deposition of Metal Carbides," Nerva Fuel Element Development Program, Summary Report - July 1966 through June 1972, Y1852 Part 4," Oak Ridge Y-12 Plant, Oak Ridge, TN, September (1973).
6. L. LYON, "Performance of (U,Zr)C-Graphite (Composite) and of (U,Zr)C (Carbide) Fuel Elements in the Nuclear Furnace 1 Test Reactor," LA-5398-MS, Los Alamos National Laboratory, Los Alamos, NM (1973).
7. D. R. KOENIG, "Experienced Gained from the Space Nuclear Rocket Program (Rover), LA-10062-H," Los Alamos National Laboratory, Los Alamos, NM (1986).
8. D. P. BUTT, D. G. PELACCIO and M. S. EL-GENK, "A Review of Carbide Fuel Corrosion for Nuclear Thermal Propulsion Applications," LA-UR-93-4136, Los Alamos National Laboratory, Los Alamos, NM (1994).
9. M. S. EL-GENK, "Nuclear Thermal Propulsion Carbide Fuel Corrosion and Key Issues Final Report," NASA CR 197533, NASA Lewis Research Center, Cleveland, OH (1994).
10. D. G. PELACCIO, M. S. EL-GENK, and D. P. BUTT, "Hydrogen Corrosion Considerations of Carbide Fuels for Nuclear Thermal Propulsion Applications," J. Prop. Power, 11, pp. 1338-1348 (1995).
11. S. V. RAJ, J. A. NESBITT and M. E. STEWART, "Development of Advanced Coatings for Nerva-Type Fuel Elements," Nuclear and Emerging Technologies for Space (NETS 2014), February 23-26, 2014, Infinity Science Center, Stennis, MS (2014).
12. S. V. RAJ, J. A. NESBITT, L. FEHRENBACHER and D. CARPENTER, "Development of Advanced Coatings for Nerva-Type Fuel Elements," Advanced Materials for Harsh Environments, MS&T 2014, Oct 12-16, 2014, Pittsburgh, PA (2014).
13. S. V. RAJ and J. A. NESBITT, "Development of Advanced Coatings for Nerva-Type Fuel Elements," Nuclear and Emerging Technologies for Space (NETS 2015), February 22-27, 2015, Albuquerque, NM (2015).
14. S. V. RAJ, M. STEWART and J. A. NESBITT, "Advanced Protective Coatings for Gr-Based Nuclear Propulsion Fuel Elements," U.S. patent 10,068,675 B1, Sept. 4, 2018.
15. S. V. RAJ, "Advanced Multilayer Protective Coatings for Graphite, Graphite-Based and Carbide-Based Substrates," LEW 20116-1, U.S. Provisional Patent Application, June 2020.
16. S. V. RAJ, J. A. NESBITT, L. FEHRENBACHER and D. CARPENTER, "Advanced Coatings Development for Nuclear Thermal Propulsion Fuel Elements," NASA TM 2016-218836, NASA Glenn Research Center, Cleveland, OH (2016).
17. S. V. RAJ, J. A. NESBITT, W. JENNINGS and P. BONACUSE, "Microstructural Observations on Advanced Multilayer Protective Coatings for Nuclear Thermal Propulsion," NASA/TM-20210021453, NASA Glenn Research Center, Cleveland, OH (2021).
18. "Properties of Graphite Grade 2160" datasheet, Mersen USA St Marys-PA Corp., Saint Marys. PA.
19. S. WEI, H. Z. HUA and X. XIANG, "Thermodynamic Analysis and Growth of Zirconium Carbide by Chemical Vapor Deposition," Phys. Procedia, 46, pp. 88-101 (2013).
20. S. S. ZUMDAHL, "Introductory Chemistry: A Foundation," (5th ed.), Houghton Mifflin Co., Boston, MA (2004).